1 Solidification Heat Transfer

The solidification problem consists of finding an absolute temperature field T at every material point ($\vec{X}$) based on the energy conservation principle

$$-\nabla \cdot \vec{q} \;=\; \rho \, \frac{\partial u}{\partial T} \, \left(\frac{\partial T}{\partial t} \;+\; \nabla T \;\cdot\; \vec{v} \right) \tag{1}$$

subject to the boundary conditions

$$T \;=\; \bar{T} \tag{2}$$

$$\vec{q} \cdot \vec{n} \;=\; q_{conv} \;+\; \bar{q} \tag{3}$$

and the initial conditions

$$T(\vec{X}, t)|_{t=0} \;=\; T_0(\vec{X}) \tag{4}$$

$$f_l(\vec{X}, t)|_{t=0} \;=\; 1 \tag{5}$$

Eq. (1) represents the thermal energy balance of a rigid heat conductor (mechanical dissipation is not considered) where the ∇ is the gradient operator with respect to the Cartesian reference system, ρ is the mass density, and u is the specific internal energy, and $\vec{v}$ is the advection velocity. The heat flux $\vec{q}$ can be related to the temperature gradient through the Fourier law of heat conduction as

$$\vec{q} \;=\; -\, k \, \nabla T \tag{6}$$

where k is the thermal conductivity. Eq. (2) represents the temperature prescribed essential boundary condition (BC), and Eq. (3) is the heat flux specified natural BC where q_{conv} is the heat flux due to convection and $\bar{q}$ is the specified heat flux. From Newton's law of cooling,

$$q_{conv} = h \, (T - T_\infty) \tag{7}$$

where h is the temperature-dependent heat transfer coefficient (HTC) and T_∞ is the atmospheric temperature. The two initial conditions considered are: $T_0(\vec{X})$ is the initial temperature, and f_l is the liquid phase fraction which is initially taken as one.

During the non-isothermal phase-changes, there exists a *mushy zone* on which the phase fraction varies from zero to one, separating the liquid and solid domain as shown in Fig. 1a. As usual, $\Omega \;= \Omega_l \cup \Omega_m \cup \Omega_s$. The phase fraction for the non-isothermal case can be stated as

$$f_l(T) = \begin{cases} 1, & T > T_l & \text{on } \Omega_\text{l} \\ 0 < g(T) \leq 1, & T_s < T \leq T_l & \text{on } \Omega_\text{m} \\ 0, & T \leq T_s & \text{on } \Omega_\text{s} \end{cases} \tag{8}$$

where $g(T)$ is the phase-change function which can be derived from the phase change kinetics. A simple approximation for this function is a linear one (as shown in Fig. 1b), given as

$$g(T) = \frac{T - T_s}{T_l - T_s}, \qquad T_s \leq T \leq T_l \tag{9}$$

The specific internal energy of a non-linear phase changing heat conductor can be stated as

$$u \;=\; \int_{T_{ref}}^{T} C_p \; dT \;+\; L \; f_l \tag{10}$$

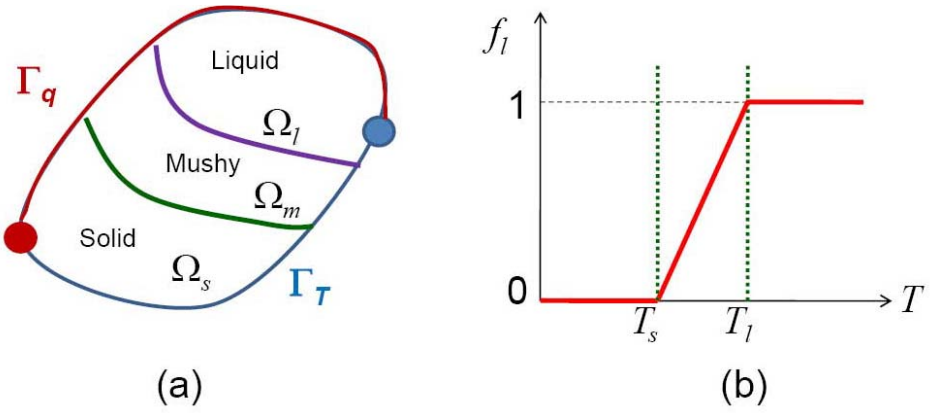

Figure 1: (a) Domain of the non-isothermal phase-change heat conductor, (b) Linear phase change function

where T_{ref} is a reference temperature, C_p is the specific heat capacity, and L is the latent heat of melting. Substituting Eq. (10), and Eq. (6) in Eq. (1) becomes

$$\nabla \cdot (k \nabla T) \;=\; \rho \left(C_p \;+\; L \, \frac{\partial f_l}{\partial T} \right) \; \left(\frac{\partial T}{\partial t} \;+\; \nabla T \;\cdot\; \vec{v} \right) \tag{11}$$

Eq. (11) contains advection term $\nabla T \;\cdot\; \vec{v}$. While writing in non-dimensional form, Eq. (11) yields the Peclet number $Pe \;=\; V L_c / \alpha$ which is very large for steel continuous casting (in the order of 200–500). In such situation, energy advection dominates energy diffusion. Therefore, with out the loss of generality, $\nabla T \;\cdot\; \vec{v}$ term can be neglected. The final form of the Governing Differential Equation (GDE) for the phase-change problem using the effective heat capacitance method [1] is given as,

$$\nabla \cdot (k \nabla T) \;=\; \rho \left(C_p \;+\; L \, \frac{\partial f_l}{\partial T} \right) \; \frac{\partial T}{\partial t} \tag{12}$$

2 Casting Simulation Model

Continuous casting of steel alloys requires following key components: tundish, submerged entry nozzle, mold, spray nozzles, etc. The model which is considered in the casting simulation addresses the heat transfer from the casting ingot to the mold, the spray regions, and the ambient. Fig. 2 shows the three dimensional curved geometry with rectangular cross-section. The reference axes are chosen in the following manner: x axis – ingot width direction, y axis – ingot thickness direction, and z axis – casting or axial direction.

Due to high Peclet number in the casting direction, heat conduction along that direction can be simply neglected. Therefore, a 2-D traveling slice approach is followed to simulate the temperature profiles during casting. The considered 2-D slice travels along the casting direction, the boundary conditions are suitably applied according to the position of the slice. Even though, the process reaches the Eulerian steady-state (with respect to the position, the temperature will not change), transient Lagrangian analysis (the material points undergo change in temperature) is attempted. Therefore, the reference frame is attached to the traveling slice. The rollers which are not shown in figure pulls the ingot constantly and make into follow a curved path with constant curvature. It can be perceived from the figure that the reference axis at the beginning of the casting is rotated

about the x axis. Due to this reason, the x and y axes interchanges when the slice moves from horizontal to vertical positions.

The assumptions involved in the model are described once again as follows:

1. The material is treated as an isotropic rigid heat conductor.
2. The liquid flow is neglected. Therefore, the liquid phase is treated as a fictitious solid.
3. Fixed grid method is followed. Therefore, the computational 2–D domain is not explicitly decomposed into solid, liquid, and mushy zones. The position of phase front and its kinetics are implicitly enforced in the energy balance.
4. The dissipation due to mechanical deformation is negligible when compared to the latent heat release.
5. The back diffusion effect is not considered. Therefore, the partition coefficient is taken as unity. The micro and macro segregations are neglected.
6. The heat generation due to the frictional dissipation at the contact interface is assumed to be negligible.
7. There is no pore formation, i.e. $f_s + f_l = 1$. Where f_s and f_l are solid and liquid volume/phase fractions, respectively.

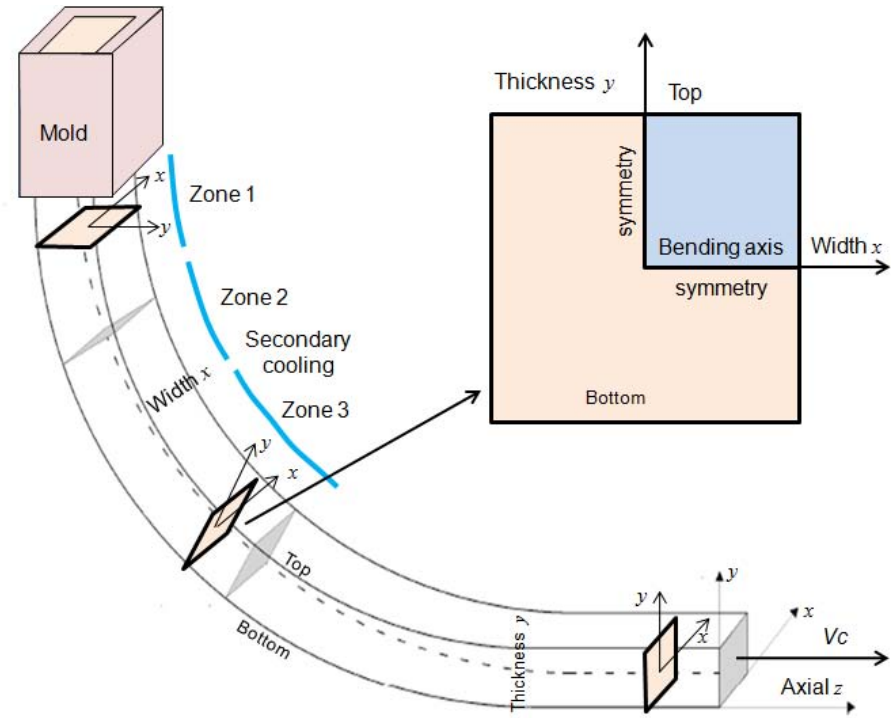

Figure 2: Schematic representation of casting simulation model

3 Boundary Conditions

3.1 Mold boundary

The quantitative analysis of mold heat transfer was presented by Brimacombe [2]. Heat transfer from the solidifying metal to the mold depends on a series of thermal resistances such as the solidifying shell, mold flux, and air gap s as shown in Fig 3. The shell and the mold flux resistances

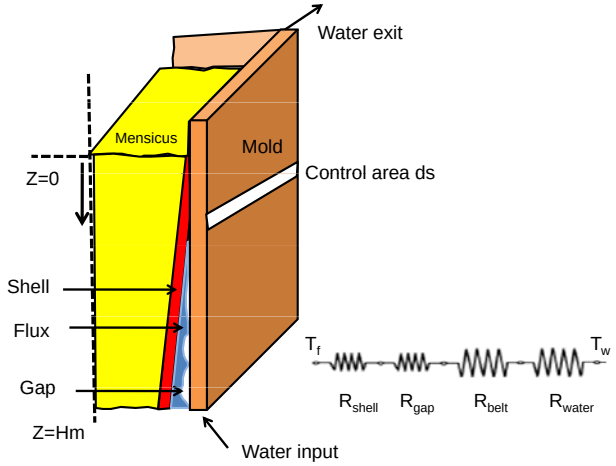

Figure 3: Schematic of the thermal resistances against heat withdrawal from mold

can be calculated from the known thermo-physical properties of the solidifying shell and slag. Mold powder or flux powder or slag that is added to the liquid steel gets melted, flows between the shell and mold and acts as a lubricant. The slag re-solidifies along the mold and acts as a resistance for the heat transfer. Meng *et al.* [3] extensively studied the behavior of the mold slag. The gap formation is unknown and difficult to predict. When thermal shrinkage of the solidifying shell is able to overcome the counteracting liquid ferro static pressure, a gap forms. The behavior of the mold slag and gap affects the overall heat transfer in the mold [2, 4, 5]. Since it is difficult to accurately model the mold behavior, there are also several practical correlations to predict the local heat flux in the mold. These correlations are obtained by measuring the temperature distribution in the mold wall.

1. Brimacombe *et al.* [6] proposed an empirical relation for the heat flux as a function of the casting speed as

$$q(W/m^2) = 2.21 \times 10^6 - 2.67 \times 10^5 \sqrt{\frac{z(m)}{V_c(m/s)}}. \tag{13}$$

2. Ha *et al.* [7] presented the heat flux in the mold as a function of casting time (s) as ,

$$q(W/m^2) = 0.07128e^{-t(s)} + 2.328e^{-t(s)/9.5} + 0.698. \tag{14}$$

3. Alizadeh *et al.* [8] presented an analytical expression for the heat flux in the mold that includes the practically controllable parameters such as mold height, cooling water flow rate

and the cooling water temperature rise. The local heat flux can be expressed as a function of the water temperature rise and the distance from the meniscus as

$$q(x,z) = A\ f(x)\ \frac{\alpha\ \rho_w\ C_{pw} Q\ \Delta T_w}{P_m}\ \frac{e^{-\alpha z}}{1-e^{-\alpha H_m}} \tag{15}$$

where α is taken as 1.25, ρ_w, C_{pw}, Q, and ΔT_w are the cooling water density, specific heat capacity, flow rate, and total water temperature rise respectively, P_m is the mold perimeter, H_m is the mold height, A is the specific mold parameter which is considered as 1.35, f is the lateral factor, and z is the axial distance from meniscus.

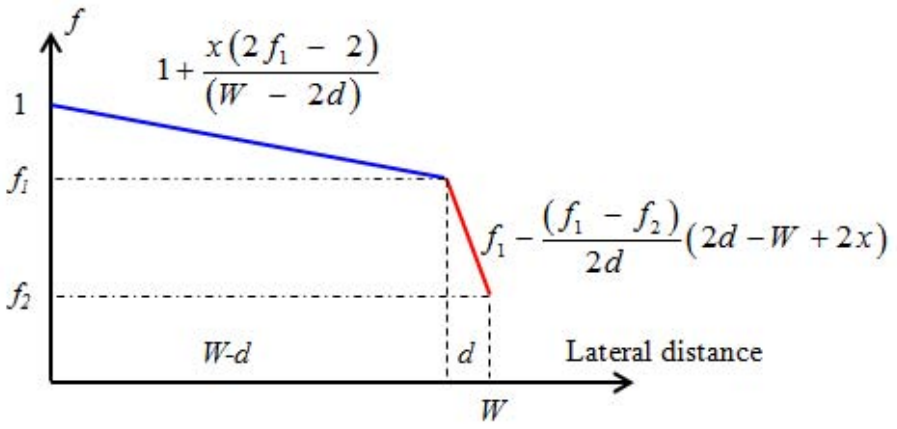

Figure 4: Alizadeh model : factor f

The variation of f is controlled by two additional parameters f_1 and f_2 as shown in Fig. 4. The mold perimeter (P_m) is modified as

$$P_m\ =\ 2\ (W-2d)\ (f_1+1)\ +\ 4d\ (f_1+f_2) \tag{16}$$

where W is the lateral dimension of the ingot, and d is the corner compensation distance which is considered as 10 mm.

4. *OVGU model* is based on the thermomechanical characteristics of the ingot and mold. When the casting speed, ingot size, and mold parameters changes, the heat flux changes. The gap dependent contact heat transfer coefficient is used to couple the thermal behavior of mold and ingot. Mold is considered as rigid body and elasto-plastic constitutive law is assumed for the solidifying ingot.

3.2 Secondary cooling

In this section, calculation of heat transfer coefficient from the water flow rate explained in detail.

3.2.1 Secondary cooling heat transfer

In the secondary cooling zone, the surface temperature of the strand is maintained above 800^o C. At these temperatures, the heat transfer occurs in the film boiling region of the boiling curve [9].

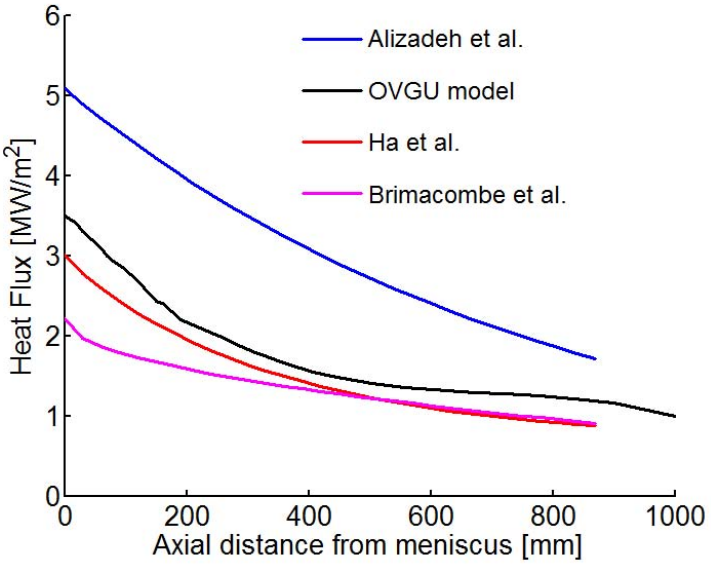

Figure 5: Mold heat flux models

In the film boiling regime, the heat extraction is a function of the water flow rate. As established by many experiments, the widely used relation for the heat transfer coefficient is expressed as [9],

$$h_{spray} = 392.5 Q_d^{0.55}(1 - 0.0075 T_w) \tag{17}$$

where Q_d is the water flow rate in l/(m^2.s) and T_w is the temperature of the cooling water [9, 10, 11]. However, Fujimoto *et al.*[12] proposed a model based on droplet diameter (D), droplet velocity (V), and number density of droplets (N) as

$$h_{spray} = M(Q_d)\ D^{1.1}\ V^{1.1}\ N^{0.65} \tag{18}$$

where M is the flow rate dependent constant as shown in Fig. 6. Droplet number density is calculated from the relation [12],

$$Q_d = \rho \frac{\pi D^3}{6}\ \ V\ N \tag{19}$$

Sauter mean diameter (d_{32}) can be given as in [13]

$$\frac{d_{32}}{d_o} = 3.67 \left[We_{d_o}^{0.5} Re_{d_o} \right]^{-0.259} \tag{20}$$

$$We_{d_o} = \frac{\rho_a v^2 d_o}{\sigma} \tag{21}$$

$$Re_{d_o} = \frac{\rho_f v d_o}{\mu_f} \tag{22}$$

$$v = \frac{2\Delta P}{\rho_f} \tag{23}$$

where d_o is the nozzle orifice diameter, ρ_a is the air density, ρ_f is the water density, σ is the surface tension, μ_f is the water dynamic viscosity, and ΔP is the pressure difference occurs in the nozzle.

From the Sauter mean diameter d_{32}, droplet diameter (D) at the impinging location is assumed in between 1.2 d_{32} at the center and 0.8 d_{32} at the outermost. The droplet velocity (V) is assumed to depend on the angle from the center of the nozzle times jet velocity (v).

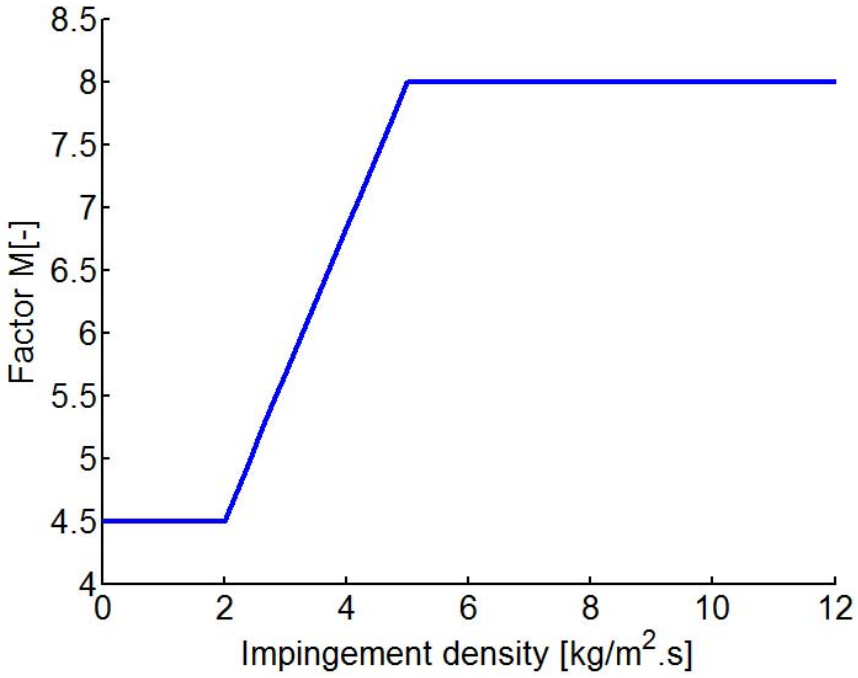

Figure 6: Schematic of the thermal resistances against heat withdrawal from mold

3.2.2 Nozzle Characteristics

Three different pressure swirl nozzles used in the plant is given in Tab. 1. The cone angle given in the table is for the standard water flow rate at the rated pressure. Pressure at different flow rates can be calculated from the relation

$$Q_1 \sqrt{P_1} = Q_2 \sqrt{P_2}$$

The cone angle and impingement density at different flow rates need experimentation. Fig. 7 shows the variation of cone angle with respect to water flow rate which is determined from the sequence of images taken during the experiment. Nearly all the three nozzles behave in a similar manner at the low flow rate.

Impingement density is measured for all the three nozzles with two different flow rates. For a single nozzle, minimum and maximum operating flow rates are considered. It is also necessary to develop a model which can predict the local impingement density for the individual nozzles. Fig. 9 shows the impingement density distribution for the zone 1 nozzle. It is observed that two different distinct zones exist: (a) core region with nearly constant impinging rate and (b) outer region with drastic reduction. Therefore, it is assumed to model the impingement density which depends on the following parameters: (a) flow rate (b) distance from the surface (c) cone angle, (d) inner radius, and (e) outer radius. Fig. 8 explains the various correlation parameters required to compute the

Zone	Nozzle	flow rate Liter/min	Pressure bar	Cone angle deg
I	100 697	3.5	2.8	65
IIa	100 688	2.5	2.8	60
IIa & III	111 672	2.0	2.8	50

Table 1: Nozzle Characteristics

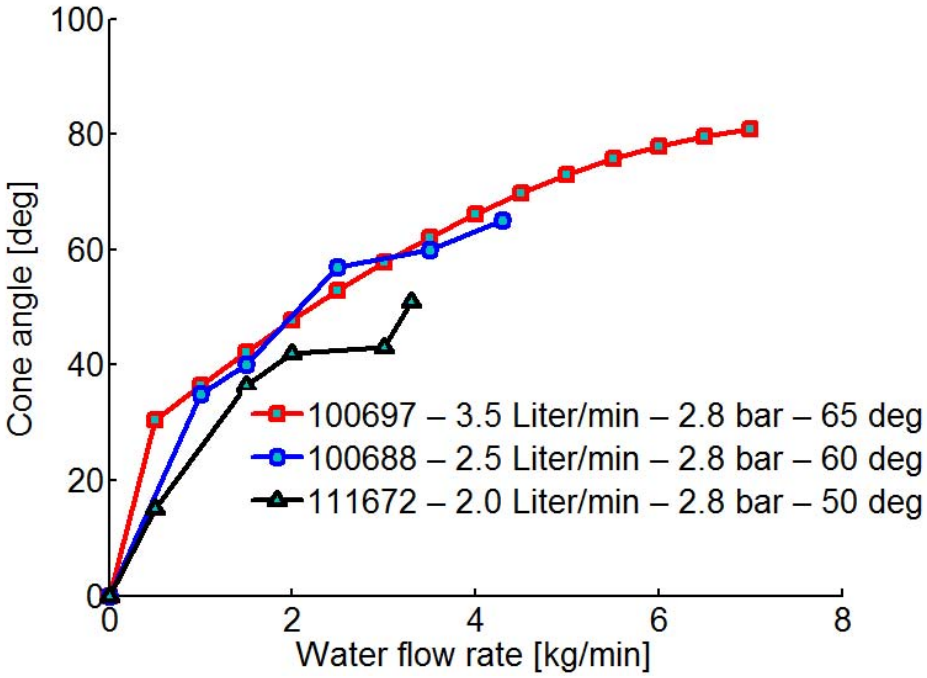

Figure 7: cone angle vs. flow rate

impingement density. However, these are just empirical relations which does not have any physical meanings.

Fig. 10 shows the zone 2 nozzle impingement density distribution. Zone 3 nozzle is operated under very low flow rate as shown in Fig. 11 due to fact that the cone development does not occur. Therefore, the impingement is very at the center. Due to the complexity in the impingement density prediction, there is a necessity to develop a theory behind it.

Along with water cooling, radiative heat transfer is also considered. The emissivity of the strand is assumed to vary with temperature as given in [14]

$$\epsilon \;=\; 0.0002\; T + 0.6274 \tag{24}$$

where T is in ^{o}C.

3.2.3 HTC matrix

In the CASTSIM, secondary cooling heat transfer coefficient (HTC) is taken from the global impingement density matrix, droplet diameter matrix, and number density matrix. Each nozzles local

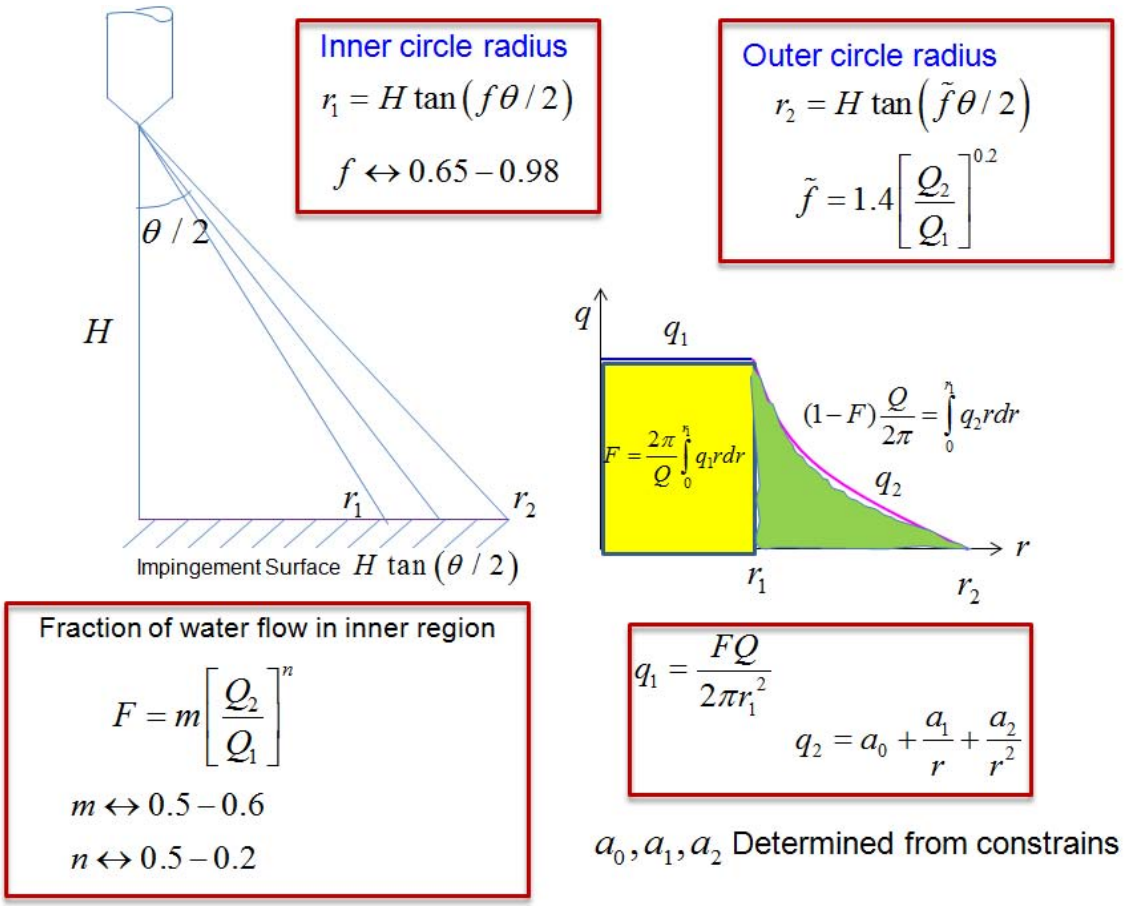

Figure 8: Correlations for the prediction of impingement density

matrix is calculated and carefully inserted in the global matrix based on the axial position. When there is an overlapping between two nozzle impingements, summation is suitably assumed. Fig. 12 shows the total flux distribution along the strand surface.

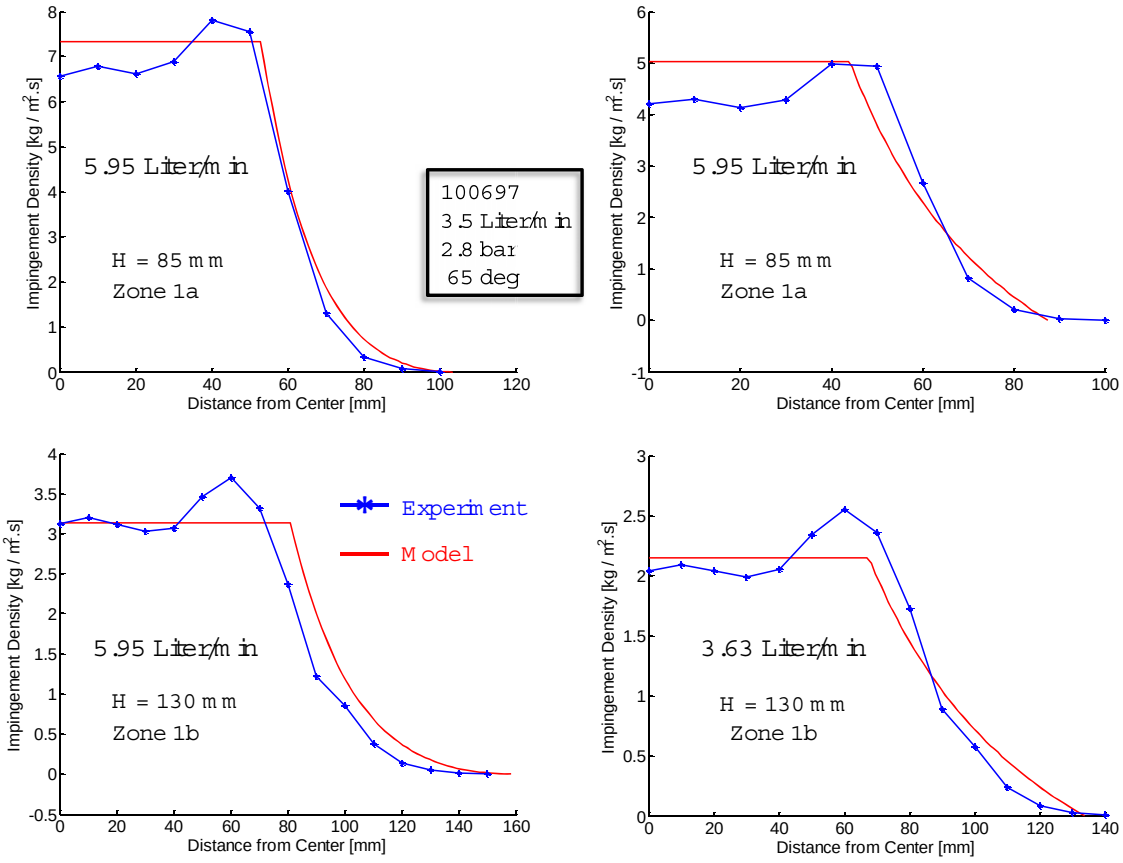

Figure 9: Impingement density : Zone 1 nozzle

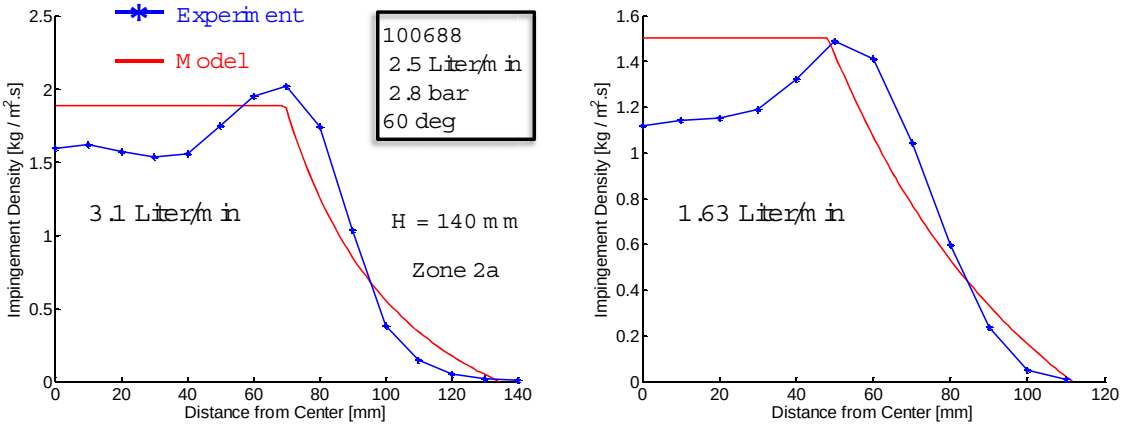

Figure 10: Impingement density : Zone 2a nozzle

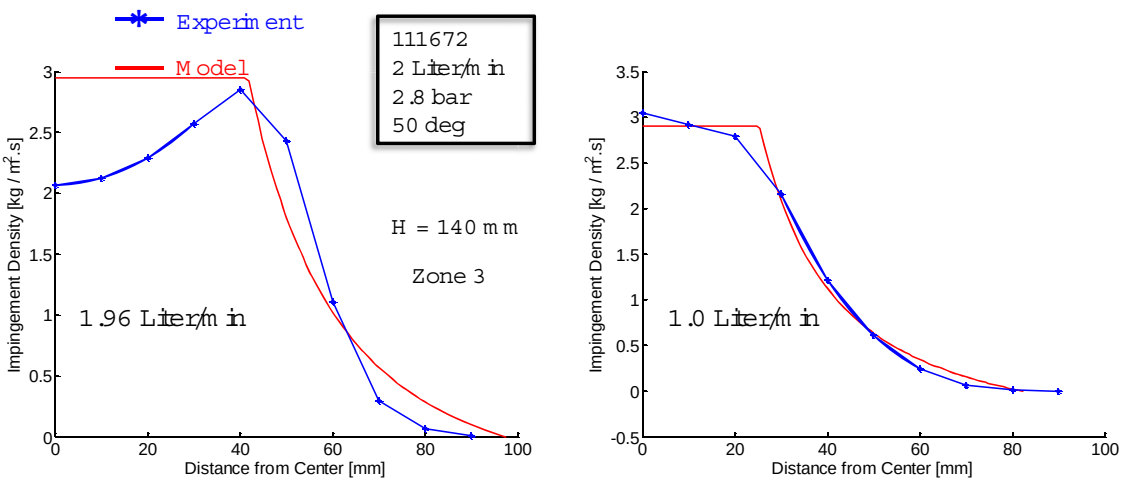

Figure 11: Impingement density : Zone 2b & 3 nozzle

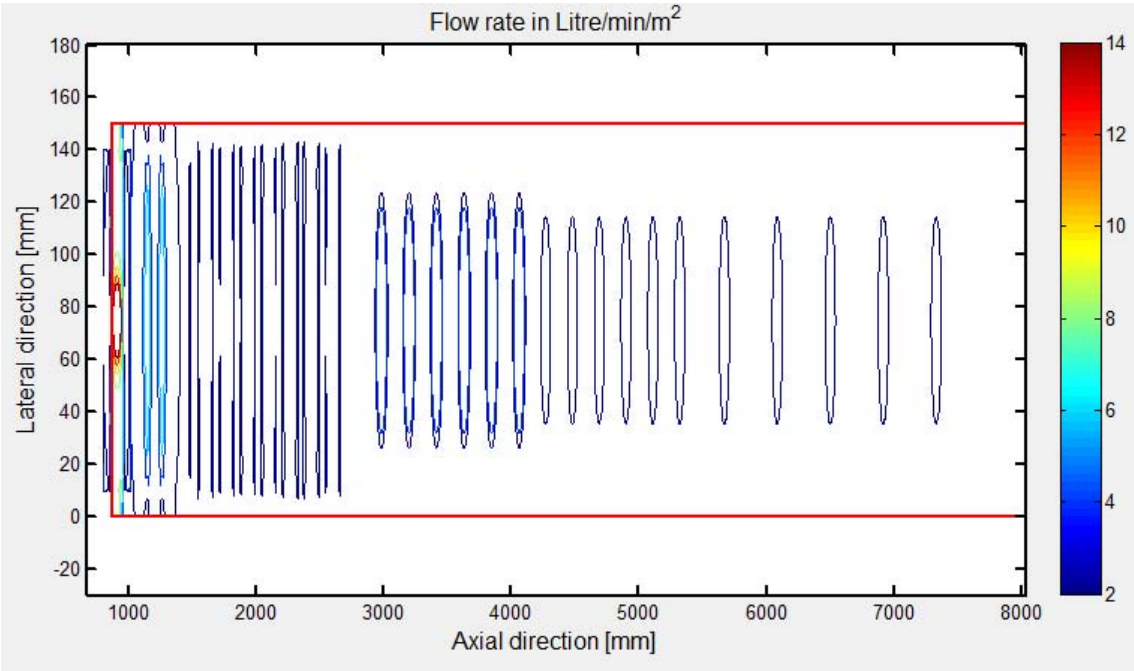

Figure 12: Impingement density along the axial distance

References

[1] D.Celentano, E.Orate, and S.Oller, "A temperature-based formulation for finite element analysis of generalized phase-change problems," *International Journal for Numerical Methods in Engineering*, vol. 37, pp. 3441–3465, 1994.

[2] J.K.Brimacombe, "Empowerment with knowledge-toward the intelligent mold for the continuous casting of steel billets," *Metallurgical Transactions B*, vol. 24B, pp. 917–935, 1993.

[3] Y.A.Meng and B.G.Thomas, "Heat-transfer and solidification model of continuous slab casting: Con1d," *Metallurgical and Materials Transactions B*, vol. 34B, pp. 685–705, 2003.

[4] B.G.Thomas, I.V.Samarasekera, and J.K.Brimacombe, "Mathematical model of the thermal processing steel ingots: Part i. heat flow model," *Metallurgical Transactions B*, vol. 18B, pp. 119–130, 1987.

[5] A.Grill, K.Sorimachi, and J.K.Brimacombe, "Heat flow, gap formation and break-outs in the continuous casting of steel slabs," *Metallurgical Transactions B*, vol. 7B, pp. 177–189, 1976.

[6] J.K.Brimacombe, P.K.Agarwal, S.Hibbins, B.Prabhakar, and L.A.Baptista in *Continuous casting vol.II : Heat flow, solidification and crack formation* (J.K.Brimacombe, I.V.Samarasekera, and J.E.Lait, eds.), pp. 109–123, 1984.

[7] J.S.Ha, J.R.Choa, B.Y.Leeb, and M.Y.Hac, "Numerical analysis of sceondary cooling and bulging in the continuous casting of steel," *Journal of Materials processing technology*, vol. 113, pp. 257–261, 2001.

[8] M.Alizadeh, A.J.Jahromi, and O.Abouali, "New analytical model for local heat flux density in the mold in continuous casting of steel," *Computational Materials Science*, vol. 44, pp. 807–812, 2008.

[9] J.Sengupta, B.G.Thomas, and M.A.Wells, "The use of water cooling during the continuous casting of steel and aluminum alloys," *Metallurgical and Materials Transactions A*, vol. 36A, pp. 187–204, 2005.

[10] G.Straffelini, L.Lutterotti, M.Tonolli, and M. Lestani, "Modeling solidification microstructures of steel round billets obtained by continuous casting," *ISIJ International*, vol. 51, pp. 1448–1453, 2011.

[11] Y.Ito, T.Murai, Y.Miki, M.Mitsuzono, and T.Goto, "Development of hard secondary cooling by high-pressure water spray in continuous casting," *ISIJ International*, vol. 51:9, pp. 1454–1460, 2011.

[12] H.Fujimoto, N.Hatta, H.Asakawa, and T.Hashimoto, "Predictable modelling of heat transfer coefficient between spraying water and a hot surface above the leidenfrost temperature," *ISIJ International*, vol. 37, no. 5, pp. 492–497, 1997.

[13] N. Mascarenhas and I. Mudawar, "Analytical and computational methodology for modeling spray quenching of solid alloy cylinders," *International Journal of Heat and Mass Transfer*, vol. 53, no. 25-26, pp. 5871–5883, 2010.

[14] C. Assuncao, R. Tavares, G. Oliveira, and L. Pereira, "Comparison of uniform and non-uniform water flux density approaches applied on a mathematical model of heat transfer and solidification for a continuous casting of round billets," *Metallurgical and Materials Transactions B*, vol. 46, no. 1, pp. 366–377, 2015.